

A machine learning approach to portfolio pricing and risk management for high-dimensional problems*

Lucio Fernandez-Arjona[†] Damir Filipović[‡]

22 May 2020

Abstract

We present a general framework for portfolio risk management in discrete time, based on a replicating martingale. This martingale is learned from a finite sample in a supervised setting. The model learns the features necessary for an effective low-dimensional representation, overcoming the curse of dimensionality common to function approximation in high-dimensional spaces. We show results based on polynomial and neural network bases. Both offer superior results to naive Monte Carlo methods and other existing methods like least-squares Monte Carlo and replicating portfolios.

keywords: Solvency capital; dimensionality reduction; neural networks; nested Monte Carlo; replicating portfolios.

1 Introduction

Financial institutions face a variety of risks on their portfolios. Whether they be market and credit risk for investment portfolios, default and prepayment risk on their mortgage portfolios, or longevity risk on life insurance portfolios, the balance sheet of a bank or insurance company is exposed to many risk factors. Failure to manage these risks can lead to insolvency—with the associated losses to shareholders, bondholders and/or customers—or overly conservative business strategies, which hurt consumers.

Alongside qualitative assessments—and plenty of common sense—portfolio risk management requires quantitative models that are accurate and sufficiently fast to provide useful information to management. Additionally, government regulations, such as solvency regimes, require extensive calculations to produce the required reports.

Simulation techniques are often used to explore possible future outcomes. Since quantitative models require to estimate conditional expectations across a time interval, Monte Carlo simulations

*We thank Antoon Pelsser for comments.

[†]University of Zurich. Email: lucio.fernandez.arjona@business.uzh.ch

[‡]EPFL and Swiss Finance Institute. Email: damir.filipovic@epfl.ch

can be used to calculate those expectations. However, Monte Carlo methods suffer from problems with both accuracy and speed.

Alternatives to Monte Carlo methods have been developed over the years, some of them using functional approximation techniques. Under this approach, an approximation to the full, slow model is built using one or more faster functions. For example, the behaviour of a portfolio can be replicated via an appropriate combination of basis functions, which are faster to calculate than the original model.

Many, if not all, of these alternatives suffer from several problems: some are not entirely data-driven—requiring subject matter expertise—which limits their applicability to complex problems and the ability to automate them, others can be automated but have low quality of the approximation, while others are limited to low-dimensional problems.

In this paper we present a model that overcomes or greatly diminishes the problems above. This model for calculating conditional expectations uses a machine learning approach to learn a suitable function from finite samples. We show how this function can be used to obtain accurate estimates of price and risk measures, focusing on practical real-world situations in terms of runtime and number of samples being used.

The learned functions are linear combinations of functional bases, of which we present several examples, including polynomials and neural networks (of the single-layer feed-forward type). In all cases, the conditional expectations are calculated in closed-form—even for neural networks—which contributes to the accuracy and speed of the solution.

We pay special attention to high-dimensional cases, which motivate the use of a special polynomial basis. In this basis, the input vector undergoes a data-driven, linear dimensionality reduction step similar to a linear neural network layer. This allows using polynomial-based replicating martingales in high-dimensional problems where full polynomial bases are unfeasible.

The solutions obtained are martingales that replicate the value processes, given as risk-neutral conditional expectations, of financial or insurance products. Drawing a parallel with the concept of a replicating portfolio, we call this approach “replicating martingale”. Replicating portfolios is a widely used method in the financial industry, which relies on building linear combinations of derivatives to approximate conditional expectations necessary for market risk calculations. Our proposed replicating martingale method is also based on linear combinations of basis functions, but these are not restricted to market risk calculations. Any risk exposure can be modelled with replicating martingales because its basis functions—polynomials or neural networks—are agnostic to the underlying risk type.

Given its regression-based nature and use of simulated samples, replicating martingales is a method of the least squares Monte Carlo (LSMC) family. It is, however, global in the time dimension, unlike LSMC methods used for American option pricing, which are local in the time dimension, that is, these require repeated, recursive regressions. Within the LSMC family of methods, replicating martingales are a regress-later method (Glasserman and Yu (2002)) given the regression is made against terminal payoffs and not against empirical conditional expectations.

We use two examples—a financial derivative and an insurance product—to perform extensive testing of the accuracy of the risk calculations based on replicating martingales. In line with existing machine learning literature, we also include extensive comparison with alternative methods, such as nested Monte Carlo and other LSMC methods. Also in line with machine learning best practices, we publish the datasets for our examples, Fernandez-Arjona and Filipović (2020). We hope that these datasets can be used by others to allow more direct comparisons between methods in future research.

1.1 Related literature

An early example of static replication via basis functions can be found in Madan and Milne (1994), that presents a framework for replication of general contingent claims. These contingent claims are modeled in a Hilbert space and the static replication problem is solved by constructing a countable orthonormal basis. The method is applied to the pricing and hedging of these contingent claims. Carriere (1996) and Longstaff and Schwartz (2001) use a sequential approximation algorithm to calculate the conditional expectations required in the valuation of options with a early exercise (like American options). The method estimates these conditional expectations from the cross-sectional information in the simulation by using least squares, which gives the method the name of least squares Monte Carlo. Andreatta and Corradin (2003) apply this idea to valuation of life insurance policies.

Glasserman and Yu (2002) were the first to make a distinction between regress-now and regress-later LSMC, the former being the direct estimation of the conditional expectation function, and the later the indirect estimation via regression against the terminal payoff of the contingent claim. Working in the context of American option pricing via approximate dynamic programming, they find that regress-later LSMC has interesting properties, among them less-dispersed estimates than regress-now LSMC.

In the area of polynomial regress-now LSMC, Broadie, Du, and Moallemi (2015) show that such regression-based methods can—asymptotically—improve the convergence rate of nested Monte Carlo methods. They provide quality comparisons against nested Monte Carlo, and a delta-gamma approach but not against regress-later methods, whereas we do.

A regress-later model based on orthonormal piecewise linear basis functions is presented in Pelsser and Schweizer (2016). Path-dependency and the resulting high-dimensional problem in long-term projections is managed via a hand-picked $A(Z)$ function to avoid the curse of dimensionality. In that framework, the basis functions are not guaranteed to have a closed form solution, whose existence depends on the choice of $A(Z)$. This function must be given to the method, and is based on expert judgement and knowledge of the problem domain. Moreover, the choice of A implies a trade-off between complexity and dimensionality—for a given target accuracy. High-dimensional $A(Z)$ functions lead to the curse of dimensionality while low-dimensional $A(Z)$ functions might be too complex to find a closed-form solution to their conditional expectations. By contrast, our framework uses a data-driven dimensionality reduction function in the parameter space instead of an arbitrary

function. In comparison to the piecewise linear model, which requires fixing a grid, neural networks are able to provide a data-driven grid for its activation functions. Regarding the quality of the approximation, Pelsser and Schweizer (2016) do not provide a quantitative metric for comparison between regress-now and regress-later models. Whereas, we provide extensive comparisons on risk metrics between these models, for both polynomial and neural network bases.

A neural network model is applied to solvency capital problem in life insurance in Castellani et al. (2018). The neural network model shows better performance than LSMC (regress-now model with polynomial basis functions) and a support vector regression model. All three models—including the neural network model—are regress-now models. By contrast, we focus on regress-later methods, which show better accuracy in the examples in addition to being better in theory.

In the field of uncertainty quantification, polynomial surrogate functions have been used for a long time to reduce the runtime of complex models. Recently, Hokanson and Constantine (2018) showed that polynomial ridge approximation can be extended to reduce dimensionality in a data-driven manner. We follow a similar approach and apply it to portfolio pricing and risk management for the first time, it seems.

Nested Monte Carlo methods for portfolio management have been studied in S.-H. Lee and Glynn (2003) and Gordy and Juneja (2010) among others. Gordy and Juneja (2010) show several methods that can reduce the computational cost of nested Monte Carlo for a homogeneous portfolio of financial instruments with an additive structure. Since we aim to cover both financial derivatives and insurance portfolios—where it is common that portfolios do not exhibit such additive structure—we restrict our comparisons to standard nested Monte Carlo.

The remainder of the paper is as follows. Section 2 formalizes the replicating martingale problem and recalls the standard nested Monte Carlo approach. Section 3 describes our machine learning approach to the replicating martingale problem. Section 4 and 5 provide numerical case studies: a European call option in Section 4, and an insurance liability model in Section 5. Section 6 concludes. The appendix contains proofs and technical background material. Section A describes the quality metrics used to compare different methods. Section B contains the economic scenario generator underlying the numerical examples in the main text. Sections C, D, and E contain proofs, and values of key parameters. Sections F and G present an analysis of the sensitivity of the proposed methods to different hyper-parameters.

2 The replicating martingale problem

We work in an economy with finite time horizon T . Randomness is modeled on a filtered probability space $(\Omega, \mathcal{F}, (\mathcal{F}_t), \mathbb{Q})$ with \mathbb{Q} being the risk-neutral measure corresponding to some numeraire. If not otherwise stated, all financial values and cash flows are discounted by this numeraire. There is an \mathbb{R}^d -valued stochastic driver process $X = (X_1, \dots, X_T)$, which is adapted to the filtration (\mathcal{F}_t) , and such that X_t is independent of \mathcal{F}_{t-1} . The physical measure is denoted by $\mathbb{P} \sim \mathbb{Q}$.

We consider an asset–liability portfolio whose discounted cash flows accumulate to the dis-

counted terminal value at T which is given as function of X ,

$$f(X) = \sum_{t=1}^T \zeta_t$$

with time- t cash flows $\zeta_t = \zeta_t(X_1, \dots, X_t) \in L_{\mathbb{Q}}^2$.

There are many examples that fit this description, such as financial derivatives, insurance liabilities, mortgage-backed instruments. Our goal is to find the gains process of the portfolio, that is, the $L_{\mathbb{Q}}^2$ -martingale given by

$$Z_t = \mathbb{E}_t^{\mathbb{Q}}[f(X)] = \underbrace{\sum_{s=1}^t \zeta_s}_{\text{cumulative CF at } t} + \underbrace{\mathbb{E}_t^{\mathbb{Q}}[\sum_{s=t+1}^T \zeta_s]}_{\text{time-}t \text{ value}},$$

where $\mathbb{E}_t^{\mathbb{Q}}[\cdot] = \mathbb{E}^{\mathbb{Q}}[\cdot \mid \mathcal{F}_t]$ denotes the \mathcal{F}_t -conditional expectation. In particular, Z_t is not given in closed form but has to be derived by simulating future cash flows. This creates many computational challenges for certain applications, as described below.

Applications: risk measurement In many insurance and banking solvency regulatory frameworks (e.g. Solvency II, Swiss Solvency Test, Basel III), capital calculations are based on the value at risk or expected shortfall of $-\Delta Z_t$, where $\Delta Z_t = Z_t - Z_{t-1}$ denotes the profit over period $[t, t+1]$, which are defined as follows:

$$\begin{aligned} \text{VaR}_{\alpha}(Y) &= \inf \{y : F_Y(y) \geq \alpha\} = F_Y^{-1}(\alpha) \\ \text{ES}_{\alpha}(Y) &= \frac{1}{1-\alpha} \int_{1-\alpha}^1 \text{VaR}_{\gamma}(Y) d\gamma, \end{aligned} \tag{1}$$

where Y is a random variable with \mathbb{P} -distribution function denoted by F_Y , and $\alpha \in (0, 1)$ denotes the confidence level.

In insurance regulation risk is normally measured for a one-year horizon and the economic capital is $\rho[-\Delta Z_1]$, where ρ is a placeholder for either VaR_{α} or ES_{α} . There are cases, however, where calculations require 3 year capital projections which would be calculated by $\rho[-\Delta Z_1]$, $\rho[-\Delta Z_2]$ and $\rho[-\Delta Z_3]$ for years one, two and three respectively.

Applications: hedging Given tradable financial instruments with gains processes G , i.e., $L_{\mathbb{Q}}^2$ -martingales, find a predictable hedging strategy ψ that approximately replicates the profit,

$$\psi_t^{\top} \Delta G_t \approx \Delta Z_t.$$

For example, ψ could minimize the local quadratic hedging error, $\min_{\psi_t} \mathbb{E}_{t-1}^{\mathbb{Q}}[|\psi_t^{\top} \Delta G_t - \Delta Z_t|^2]$, so that

$$\psi_t = \mathbb{E}_{t-1}^{\mathbb{Q}}[\Delta G_t \Delta G_t^{\top}]^{-1} \mathbb{E}_{t-1}^{\mathbb{Q}}[\Delta G_t \Delta Z_t].$$

In a real-world setting, both applications mentioned above require computing $Z_t = \mathbb{E}_t^{\mathbb{Q}}[f(X)]$, which is subject to restrictions on the available computing budget, since the cumulative cash-flow function f might be very costly to evaluate.

2.1 Standard nested Monte Carlo approach

Approximating the integrals in (1) via a Monte Carlo simulation is the standard method for calculating risk metrics. However, in many cases this method cannot be used in practice due to the large computational effort required. We refer to as standard nested Monte Carlo to the following process: the outer stage of the simulation consists of a set of n_0 simulations, $X_{1:t}^{(i)}$, $i = 1, \dots, n_0$, that are independent and identically distributed according to the distribution μ of the risk factors until the time t of the risk calculation horizon. The portfolio value $Z_t^{(i)}$ and associated portfolio loss $\Delta Z_t^{(i)}$ for each scenario $X_{1:t}^{(i)}$ is estimated via the inner stage of Monte Carlo simulation by taking the sample mean of the n_1 inner simulations drawn for each outer simulation $X_{1:t}^{(i)}$. This is illustrated in Figure 1. Once the empirical distribution for $\Delta Z_t^{(i)}$ has been obtained, the desired risk metric is approximated via its empirical equivalent.

3 Machine learning approach

For our model, we apply the following machine-learning approach, that can be divided in two steps:

- **Approximate** f by some f^* in L^2_{μ} for which $\mathbb{E}_t^{\mathbb{Q}}[f^*(X)]$ is given in closed form.¹
- **Learn** f^* from a finite sample x_1, \dots, x_n and corresponding $f(x_1), \dots, f(x_n)$, obtaining \hat{f} .

3.1 Finite-dimensional approximation

Feature map Let \mathcal{A} be a parameter set such that, for every $A \in \mathcal{A}$, there are m linearly independent functions $\phi_{A,1}, \dots, \phi_{A,m}$ in L^2_{μ} . These functions form the feature map $\phi_A = (\phi_{A,1}, \dots, \phi_{A,m})^{\top}$. For each function $\phi_{A,i}$ its expectation $\mathbb{E}_t^{\mathbb{Q}}[\phi_{A,i}(X)]$ is known in closed form. This last requirement is necessary for the one of the key distinguishing factors between the model proposed here and other models in the literature: we obtain the gains process of the portfolio by regressing against its terminal value. Our model, therefore, falls within the “regress later” category first mentioned in Glasserman and Yu (2002). As we will see in Section 4, this approach performs much better than the alternative “regress now”.

For every $A \in \mathcal{A}$, the L^2_{μ} -projection of f on $\text{span } \phi_A$ is given by $f_A = \phi_A^{\top} \beta_A$, for the unique minimizer

$$\beta_A = \arg \min_{\beta \in \mathbb{R}^m} \|f - \phi_A^{\top} \beta\|_{L^2_{\mu}} = \langle \phi_A, \phi_A^{\top} \rangle_{L^2_{\mu}}^{-1} \langle \phi_A, f \rangle_{L^2_{\mu}}. \quad (2)$$

In the particular case where $\phi_{A,1}, \dots, \phi_{A,m}$ are orthonormal in L^2_{μ} then the Gram matrix $\langle \phi_A, \phi_A^{\top} \rangle_{L^2_{\mu}} = I_m$, so that $\beta_A = \langle \phi_A, f \rangle_{L^2_{\mu}}$

¹ f^* is also called surrogate function, e.g., in Hokanson and Constantine (2018).

Feature learning Having described the feature map in our regression model, we point out that the features themselves are also learned from the data. This is the second key distinguishing factors of our model in comparison to others: we tackle the curse of dimensionality that comes naturally with regress-later models by learning a reduced set of features. To do this, we minimize the approximation error $\|f - f_A\|_{L_\mu^2}$ over $A \in \mathcal{A}$. We assume that there exists an optimal parameter $(A^*, \beta^*) \in \mathcal{A} \times \mathbb{R}^m$ attaining the **best approximation error**

$$\min_{(A, \beta) \in \mathcal{A} \times \mathbb{R}^m} \|f - \phi_A^\top \beta\|_{L_\mu^2} = \|f - \phi^{\star\top} \beta^*\|_{L_\mu^2} \quad (3)$$

where we have $\beta^* = \beta_{A^*}$, by (2), and we write $\phi^* = \phi_{A^*}$, for short. Our goal of approximating f is achieved by the best L_μ^2 -projection

$$f^* = \phi^{\star\top} \beta^* = f_{A^*}$$

Approximate gains process If for each $\phi_{A,i}$, we have $\mathbb{E}_t^{\mathbb{Q}}[\phi_{A,i}(X)]$ given in closed form then we also have the approximate gains process in closed form,

$$Z_t^* = \mathbb{E}_t^{\mathbb{Q}}[\phi^*(X)]^\top \beta^*, \quad (4)$$

and the best approximation error carries over,

$$\begin{aligned} \|Z_t - Z_t^*\|_{L_\mathbb{Q}^2} &\leq \|f - \phi^{\star\top} \beta^*\|_{L_\mu^2}, \\ \|Z_t - Z_t^*\|_{L_{\mathbb{P}}^1} &\leq \|\frac{d\mathbb{P}}{d\mathbb{Q}}\|_{L_\mathbb{Q}^2} \|f - \phi^{\star\top} \beta^*\|_{L_\mu^2} \end{aligned}$$

The expectations $\mathbb{E}_t^{\mathbb{Q}}[\phi_{A,i}(X)]$ depend on the form of $\phi_{A,i}(X)$. In our model, of which we present several examples in the following subsections, we work with ϕ_A that factorize as

$$\phi_{A,i}(X) = g_i(A^\top \underline{X}), \quad i = 1, \dots, m$$

for some functions $g_i : \mathbb{R}^p \rightarrow \mathbb{R}$ and $Td \times p$ -matrix $A = (A_1, \dots, A_p) \in \mathcal{A} \subset \mathbb{R}^{Td \times p}$, for some $p \in \mathbb{N}$. Since we work with $X \in \mathbb{R}^{T \times d}$, we add for convenience $\underline{X} \in \mathbb{R}^{Td}$, a flat version of X such that $\underline{X}_{(t-1)d+j} = X_{t,j}$. This allows us to easily express the role of A as a linear map that creates features and performs a key role in driving the dimensionality reduction that we seek in high dimensional problems. For the expectations, we then obtain

$$\mathbb{E}_t^{\mathbb{Q}}[\phi_{A,i}(X)] = \mathbb{E}_t^{\mathbb{Q}} \left[g_i \left(\sum_{s=1}^{td} (A^\top)_s \underline{X}_s + \sum_{s'=td+1}^T (A^\top)_{s'} \underline{X}_{s'} \right) \right] = G_{t,i}(\mu_t) \quad (5)$$

for the function $G_{t,i}(\mu) = \mathbb{E}^{\mathbb{Q}} \left[g_i \left(\mu + \sum_{s'=td+1}^T (A^\top)_{s'} \underline{X}_{s'} \right) \right]$, where $\mu_t = \sum_{s=1}^{td} (A^\top)_s \underline{X}_s$ and we write $(A^\top)_s$ for the s th column vector of A^\top .

3.2 Full polynomial bases

Let $\mathcal{A} = \{\mathbf{I}_{Td}\}$, so that $|\mathcal{A}| = 1$, and write $\phi_A \equiv \phi$, for short, so that also $\phi = \phi^*$. In this case, problem (3) reduces, and is identical, to (2). Let the feature map ϕ be composed of all polynomials of maximal degree δ or less,

$$\text{Pol}_\delta(\mathbb{R}^{Td}) = \text{span}\{x^\alpha \mid \alpha \in \mathbb{N}_0^{Td}, |\alpha| \leq \delta\}.$$

This example then matches a polynomial regress-later model. The feature map suffers the curse of dimensionality from the rapid growth of the number of basis functions m as a function of d and T ,

$$m = \dim \text{Pol}_\delta(\mathbb{R}^{Td}) = \binom{Td+\delta}{Td}.$$

If, for example, $d = 3$, $\delta = 3$, then we have

$$m = \begin{cases} 816, & \text{for } T = 5, \\ 302,621, & \text{for } T = 40. \end{cases} \quad (6)$$

Expectations under full polynomial bases The expectation at time 0, Z_0 , which corresponds to the present value or $t = 0$ price, is simply given by β_1 , the coefficient associated to the monomial of order 0.

The exact form of the conditional expectation $\mathbb{E}_t^\mathbb{Q}[\phi(X)^\top \beta] = \mathbb{E}_t^\mathbb{Q}[\phi(X)]^\top \beta$ depends on the choice of ϕ and the distribution of X . Choosing an orthogonal basis in L_μ^2 can greatly simplify the calculations. For example, for a multivariate normal $\underline{X} \sim N(0, \mathbf{I}_{Td})$ we work below with a Hermite polynomial basis.

Consider the Hermite polynomials H_1, \dots, H_m on \mathbb{R}^{Td} of degree δ or less. The multivariate (probabilists') Hermite polynomial of order α on variable \underline{X} can be expressed in terms of univariate Hermite polynomials on \underline{X}_j : $H_\alpha(\underline{X}) = \prod_{j=1}^{Td} H_{\alpha_j}(\underline{X}_j)$ where $\alpha \in \mathbb{N}_0^{Td}$. From this expression we can see that the sequence $\{H_i\}_{i=1}^m$ is not unique but depends on the mapping $i \mapsto \alpha^i$ between the natural numbers i and the multi-index α^i in order to be able to assign a unique order. Once an order is given, $\{H_i\}_{i=1}^m$ can be mapped to a subset of $\{H_\alpha\}_{\alpha \in \mathbb{N}_0^{Td}}$ such that we can write $H_i = H_{\alpha^i}$.

Under these conditions we can obtain a closed-form solution to the expectation of the feature map:

$$\begin{aligned} \mathbb{E}_t^\mathbb{Q}[\phi_i(X)] &= \mathbb{E}_t^\mathbb{Q}[H_{\alpha^i}(\underline{X})] = \prod_{j=1}^{td} H_{\alpha_j^i}(\underline{X}_j) \prod_{j=td+1}^{Td} \mathbb{E}^\mathbb{Q}[H_{\alpha_j^i}(\underline{X}_j)] \\ &= \prod_{j=1}^{td} H_{\alpha_j^i}(\underline{X}_j) \prod_{j=td+1}^{Td} 1_{\alpha_j^i=0} \end{aligned}$$

which is an explicit expression of the form (5).

3.3 Polynomials and linear dimensionality reduction

Let us consider a more general case now. In this example we fix $p \leq Td$, a degree $\delta \geq 1$ and a polynomial basis q_1, \dots, q_m of $\text{Pol}_\delta(\mathbb{R}^p)$ with

$$m = \dim \text{Pol}_\delta(\mathbb{R}^p) = \binom{p+\delta}{p}.$$

For any $A \in \mathbb{R}^{Td \times p}$ with full rank define the polynomials $\phi_{A,i} \in \text{Pol}_\delta(\mathbb{R}^{Td})$ by

$$\phi_{A,i}(x) = q_i(A^\top x), \quad i = 1, \dots, m$$

The following theorem shows that without loss of generality we can assume that A lies in the Stiefel manifold, the set of all orthonormal p -frames in \mathbb{R}^{Td} , given by

$$V_p(\mathbb{R}^{Td}) = \{A \in \mathbb{R}^{Td \times p} \mid A^\top A = \mathbf{I}_p\}.$$

Theorem 1. *For any $A \in \mathbb{R}^{Td \times p}$ with full rank, there exists $\tilde{A} \in V_p(\mathbb{R}^{Td})$ with $\text{span } \phi_A = \text{span } \phi_{\tilde{A}}$.*

Let us henceforth assume $\underline{X} \sim N(0, \mathbf{I}_{Td})$, that is, \underline{X} is Gaussian white noise. As a consequence, $A^\top \underline{X} \sim N(0, \mathbf{I}_p)$ for any $A \in V_p(\mathbb{R}^{Td})$. Accordingly, we consider the Hermite polynomials H_1, \dots, H_m on \mathbb{R}^p of degree δ or less. For any $A \in V_p(\mathbb{R}^{Td})$ we can define the polynomials

$$\phi_{A,i}(X) = H_i(A^\top \underline{X}) = H_{\alpha^i}(A^\top \underline{X}), \quad i = 1, \dots, m$$

The optimization problem (3) corresponds to **linear dimensionality reduction** with matrix manifold $V_p(\mathbb{R}^{Td}) \times \mathbb{R}^m$ in the spirit of Cunningham and Ghahramani (2015).

We can appreciate the effect of the dimensionality reduction when we compare the number of parameters for $d = 3$, $\delta = 3$, $p = 3$. In this case $\dim V_p(\mathbb{R}^{Td}) = Tdp - \frac{1}{2}p(p+1)$ and $m = \dim \text{Pol}_\delta(\mathbb{R}^p) = \binom{p+\delta}{p} = 20$, so that

$$\text{number of parameters} = \begin{cases} 9 + 20 = 29, & \text{for } T = 5, \\ 114 + 20 = 134, & \text{for } T = 40. \end{cases}$$

Compare this example to the corresponding one using the full polynomial basis (6). In the high dimensional cases of maturity $T = 40$, we now have 134 vs 302,621 parameters, thus achieving a high degree of dimensionality reduction in the parameter space.

Expectations under linear dimensionality reduction of a polynomial basis The expectation at time 0, Z_0 , which corresponds to the present value or t_0 price, is simply given by β_1 , the coefficient associated to the monomial of order 0.

As with the full polynomial basis, the expectation is shown below for a Hermite polynomial basis and multivariate normal $\underline{X} \sim N(0, \mathbf{I}_{Td})$. For more details and the full derivation of these results, we refer to Appendix D. Specifically, applying Lemma 3 we obtain

$$\mathbb{E}_t[\phi_{A,i}(X)] = \mathbb{E}_t \left[\prod_{j=1}^p H_{\alpha_j^i} \left(\sum_{s=1}^{Td} \underline{X}_s A_{sj} \right) \right] = \prod_{j=1}^p \sigma[W_j^-]^{\alpha_j^i} H_{\alpha_j^i} \left(\frac{W_j^-}{\sigma[W_j^-]} \right) \quad (7)$$

where

$$W_j^- = \sum_{s=1}^{td} A_{sj} \underline{X}_s, \quad \sigma[W_j^-] = \sqrt{\sum_{s=1}^{td} A_{sj}^2},$$

which is an explicit expression of the form (5).

3.4 Neural networks

In this third example of basis functions, we consider a one-layer neural network, which can be represented as feature map ϕ_A as follows.² We choose the activation “ReLU” function $t \mapsto t^+$ and set $\phi_{A,i}(X) = (A_i^\top \underline{X})^+$.

Remark. *Here we cannot assume that $A \in V_p(\mathbb{R}^{Td})$ as we did in Theorem 1. Indeed, consider for example $A = \begin{pmatrix} 1 & 1 \\ 0 & 1 \end{pmatrix}$, so that the “orthogonalization” is $\tilde{A} = A(A^\top A)^{-1/2} = \begin{pmatrix} 1 & 0 \\ 0 & 1 \end{pmatrix}$. Matrix A gives the feature map $\phi_A(x) = (x_1^+, (x_1 + x_2)^+)^{\top}$, while \tilde{A} gives $\phi_{\tilde{A}} = (x_1^+, x_2^+)^{\top}$. Now observe that $(x_1 + x_2)^+$ is not in the linear span of x_1^+ and x_2^+ . Hence the analog of Theorem 1 does not apply for neural networks, in general.*

For notational convenience we adopt the common practice in neural network literature of working with augmented A and \underline{X} , appending constant terms to avoid carrying explicit bias terms. For \underline{X} this means adding a constant term in the first position, $\underline{X}_0 = 1$. This additional term in \underline{X} requires an additional row in A as the new first row which holds the bias terms in the hidden layer. This makes $A \in \mathbb{R}^{(Td+1) \times p}$, where p is the number of hidden nodes. The remaining bias term, the one in the output layer, corresponds to the parameter β_{p+1} , and we have $m = p + 1$. In order to produce a constant term that matches this bias term, we append an additional constant row to A , $(1, 0, \dots, 0)$. This means that as a parameter A is in effect $(Td + 1) \times p$ -dimensional, but in actual computations $A \in \mathbb{R}^{(Td+1) \times (p+1)}$, with the following block structure:

$$\begin{pmatrix} b_1 & \dots & b_p & 1 \\ & & 0 & \\ A' & & \vdots & \\ & & 0 & \end{pmatrix},$$

where $A' \in \mathbb{R}^{(Td) \times p}$ is the core A matrix without augmentation and b_1, \dots, b_p are the bias terms of the hidden layer.³

²From a financial engineering point of view, the feature map can be thought as a portfolio of Gaussian call options.

³Strictly speaking, we ignore those A for which $\phi_{A,1}, \dots, \phi_{A,p+1}$ are not linearly independent. However, in practice this is not relevant, as the set of such singular A 's has Lebesgue measure zero in $\mathbb{R}^{(Td+1) \times (p+1)}$.

Expectations under neural network bases The expectation at time 0, Z_0 , which corresponds to the present value or t_0 price, is simply given by β_{p+1} , the bias coefficient in the output layer. The conditional expectation $\mathbb{E}_t^{\mathbb{Q}}[\phi_A(X)^\top \beta]$ is provided in the following lemma (Fernandez-Arjona (2019)).

Lemma 1. *Assume $\underline{X} \sim N(0, I_{Td})$. Then the above one-layer neural network,*

$$f^*(X) = \sum_{i=1}^{p+1} \beta_i \phi_{A,i}(X) = \sum_{i=1}^{p+1} \beta_i (A_i^\top \underline{X})^+,$$

has conditional expectation given by

$$\mathbb{E}_t^{\mathbb{Q}}[f^*(X)] = \sum_{i=1}^p \beta_i E_i(t) + \beta_{p+1},$$

where

$$E_i(t) = \mathbb{E}_t^{\mathbb{Q}} \left[(A_i^\top \underline{X})^+ \right] = \frac{1}{2} \sigma_i(t) \sqrt{\frac{2}{\pi}} \exp \left(-\frac{\mu_i(t)^2}{2\sigma_i(t)^2} \right) + \mu_i(t) \left(1 - \Phi \left(-\frac{\mu_i(t)}{\sigma_i(t)} \right) \right) \quad (8)$$

with

$$\begin{aligned} \mu_i(t) &= \mathbb{E}_t^{\mathbb{Q}} \left[A_i^\top \underline{X} \right] = \sum_{s=0}^{td} \underline{X}_s A_{si}, \\ \sigma_i(t) &= \sigma_t^{\mathbb{Q}} \left[A_i^\top \underline{X} \right] = \sqrt{\sum_{s=td+1}^{Td} A_{si}^2}, \end{aligned}$$

which is an explicit expression of the form (5).

3.5 Finite-sample estimation

Given a sample $(x_1, y_1), \dots, (x_n, y_n)$ where X is drawn from $\mu(dx)$ and $y_i = f(x_i)$, and given $A \in \mathcal{A}$, we can construct $\Phi_A \in \mathbb{R}^{n \times m}$ by $\Phi_{A,ij} = \phi_{A,j}(x_i)$.

Assuming that $m \leq n$ and $\Phi_A^\top \Phi_A$ is invertible ($\text{rank } \Phi_A = m$), the empirical version of (2) reads as the ordinary least squares (OLS) problem

$$\hat{\beta}_A = \arg \min_{\beta \in \mathbb{R}^n} \|y - \Phi_A \beta\|_{\mathbb{R}^n} = (\Phi_A^\top \Phi_A)^{-1} \Phi_A^\top y \quad (9)$$

Remark. *The law of large numbers implies, for a fixed $A \in \mathcal{A}$ and for $n \rightarrow \infty$,*

$$\hat{\beta}_A = (\frac{1}{n} \Phi_A^\top \Phi_A)^{-1} (\frac{1}{n} \Phi_A^\top y) \xrightarrow{p} \langle \phi_A, \phi_A^\top \rangle_{L_\mu^2}^{-1} \langle \phi_A, f \rangle_{L_\mu^2} = \beta_A \quad (10)$$

Finite-sample feature learning The empirical version of (3) reads as follows: we assume that there exists an optimal parameter $(\hat{A}, \hat{\beta}) \in \mathcal{A} \times \mathbb{R}^m$ such that $\Phi_{\hat{A}}^\top \Phi_{\hat{A}}$ is invertible (rank $\Phi_{\hat{A}} = m$) and attaining the best approximation error

$$\min_{(A, \beta) \in \mathcal{A} \times \mathbb{R}^m} \|y - \Phi_A \beta\|_{\mathbb{R}^n} = \|y - \Phi_{\hat{A}} \hat{\beta}\|_{\mathbb{R}^n} \quad (11)$$

where we have $\hat{\beta} = \hat{\beta}_{\hat{A}}$, by (9). Writing $\hat{\phi} = \phi_{\hat{A}}$, we obtain the estimated approximation $\hat{f} = \hat{\phi}^\top \hat{\beta}$ of f .

4 European call option example

Having presented the theoretical background, we now turn to a first example to show how the ideas in Section 3 can be used to construct a replicating martingale and how these compare to alternative approaches. In order to introduce this example, and the estimator quality metrics to be used, we begin in the next section showing how the capital calculations are performed using nested Monte Carlo.

4.1 Nested Monte Carlo

In this example, we calculate the present value (Z_0) and expected shortfall of $-\Delta Z_1$ for an European call on an equity index. We assume that we hold a short position in this call and therefore focus on the loss-making tail, that is, the tail where the equity index values are higher. In keeping with industry convention, the present value and expected shortfall are reported as positive numbers, without taking into account the fact that it is a short position.

The economic scenario generator is described in Appendix B. That generator maps X to a vector of economic factors. This vector contains several components, among them the equity index and the cash account. We will call these components EQ_t and C_t respectively. The European call payoff at time T will be

$$\max(EQ_T - K, 0)$$

and therefore

$$Z = -\max(EQ_T - K, 0)/C_T$$

where K is the strike of the option and T its maturity. The variables EQ_t , C_t , and K represent nominal—undiscounted—values.

In this example we work with two maturities $T = 5$ and $T = 40$ and for both $K = 100$ —that is, the option is at the money at time zero. The model has 3 stochastic drivers, $d = 3$, and therefore there are 15 and 120 total dimensions—individual stochastic variables—for $T = 5$ and $T = 40$, respectively.

To establish the benchmark value—the closest we can get to the “ground truth” without having a closed form solution—we first run a very large nested Monte Carlo simulation (henceforth nMC),

with 1,000,000 outer simulations (n_0) and 100,000 inner simulations (n_1). We then calculate the 99% expected shortfall on the loss-making tail. When working with an empirical distribution, as we do here based on simulation data, the expected shortfall reduces to simply averaging the 1% worst results.

Before we can test the quality of nMC estimator for a finite simulation budget, we need to decide how to split said budget between inner and outer simulations. Different combinations of outer and inner simulations will produce different nMC estimators. The bias and variance of the nested Monte Carlo estimator depends on both the amount of outer and inner simulations. Each combination has a different bias and variance and therefore a different mean absolute error. This is shown in Tables 1 and 2 for a fixed total budget of 50,000 simulations. In each individual estimation (inner–outer combination), the error is calculated as a percentage of the benchmark value and therefore we refer to the quality metric as “MApE”, for Mean Absolute percentage Error. The formula is described in Appendix A. It is important to note that since the expected shortfall is calculated on $-\Delta Z_1$, the error on Z_0 is also part of the error on $ES(-\Delta Z_1)$.

As described in Broadie, Du, and Moallemi (2015), it is not possible, in general cases, to decide for a finite budget how to make this inner-outer split in an optimal way. In this paper we will err on the side of presenting optimistic risk figures for nMC estimations, by choosing an optimal split based on our knowledge of the benchmark value. This bias towards more accurate nMC risk estimations than possible in practice will not be a problem for our analysis, since we find that the proposed replicating martingale method produces more accurate results than the optimal nMC, which is already better than what one would obtain in practice. Since the optimal number of simulations for risk calculations is different than for the pricing calculations, it is not possible to be optimal for both at the same time. We have chosen the optimal set for risk calculations. This problem does not exist for regression-based methods, since it is not necessary to split the training budget.

The effect on the present value calculations of using the split which is for optimal for risk calculations can be seen in Table 3. There, for example, the error on the 5 year call is 1.7% while in Table 1 we can see that the error would be 0.6% when using the split optimal for present value calculations—which corresponds to flat, not nested, Monte Carlo.

In order to select the optimal outer-inner combination, each combination is run 100,000 times to be able to estimate its MApE ES. The combination with the lowest MApE ES is chosen as the optimal for that (total) sample size. Table 3 shows the relationship between the MApE ES of the optimal combination and the total sample size. We can see that the estimation of $ES[\Delta Z_1]$, performed via nested Monte Carlo, is much more affected by the increased dimensionality of the problem than the estimation of Z_0 .

These Monte Carlo results will be used throughout the paper as one of the reference methods against which we measure the proposed methods. Even if the limitations of standard nested Monte Carlo mean that it is not the main approach used by practitioners in large-scale problems, it remains the simplest way to approach the estimation of conditional expectations, and it provides a

common baseline that both practitioners and academics can easily understand. In order to provide a comparison with other methods widely used in practice, we also include regress-now methods in all examples.

4.2 Applying replicating martingales

We now apply the functional bases described in Sections 3.2, 3.3, and 3.4. For each functional base we show the same quality metrics as in Section 4.1 in order to compare to the results from nested Monte Carlo estimation.

Additionally, each functional base is also compared to other related methods, such as regress-now LSMC. When comparing between regression-based methods, we use an additional quality metric: the mean L_1 error over the empirical distribution of ΔZ_1 . This metric allows us to make comparisons of the goodness-of-fit along the entire distribution, not only the tail. This metric is related to the upper bound on the error for any tail metric, not only the 1% tail used in the expected shortfall error examples. For more details about the quality metrics use, we refer to Appendix A.

4.2.1 Full polynomial bases

The first comparison uses the full polynomial basis described in Section 3.2. In Tables 4 and 5 we present the MApE comparison among Monte Carlo, regress-now polynomial basis and the replicating martingale full polynomial basis. Table 4 shows results for the present value and Table 5 for the expected shortfall estimators.

We can see how the replicating martingale outperforms the other two methods in the estimation of the present value and the 99% expected shortfall. For a more comprehensive comparison, we look at the mean L_1 error in Table 6. We can see that Table 5 confirms the conclusions from Table 6: the replicating martingale estimators outperform the regress-now estimators. In this regard, we verify what others in the literature have reported before for regress-later estimators.

Tables 4 and 5 do not show results for the full polynomial basis under the replicating martingale approach for $T = 40$. The reason for this is the combinatorial explosion in the number of basis functions as the dimensionality of the problem grows. As shown in (6), the number of basis functions for $d = 3, \delta = 3, T = 40$ is 302,621. The number of samples would have to be at least of that magnitude, yielding a problem that, while feasible for some algorithms, is not necessarily practical in the real world. Our focus is to describe a method that shows good quality even for high-dimensional problem with a manageable number of samples. It is important to note that the regress-now approach does not suffer from this problem and shows a quality improvement over the Monte Carlo approach.

4.2.2 Polynomials and linear dimensionality reduction

The problems with high dimensional cases described in the previous paragraph motivate our use of linear dimensionality reduction (LDR). As described in Section 3.3, the number of parameters to

be estimated can be greatly reduced, from 816 to 29 for $T = 5$ and from 302,621 to 134 for $T = 40$. Whether a function f can be well approximated by a polynomial basis with linear dimensionality reduction for a small δ and p depends on the nature of the function. Asymptotically, any function in $L2_\mu$ can be approximated with arbitrary precision.

The optimization problem in (11) is solved over the product manifold $V_k(\mathbb{R}^{Td}) \times \mathbb{R}^m$ rather over $\mathbb{R}^{Td \times k} \times \mathbb{R}^m$, supported by Theorem 1. This reduces the effective dimensionality of the problem and simplifies the calculation of the conditional expectation of $\phi(X)$ in Equation (4). For these examples we have used the Riemannian BFGS algorithm from Huang, Gallivan, and Absil (2015) using the C++ library published by the authors. Additionally, we tested another two algorithms, Riemannian Trust Regions (Absil, Baker, and Gallivan (2007)) as implemented by the Python library “pymanopt” (Townsend, Koep, and Weichwald (2016)), and Grassmann Gauss-Newton (Hokanson and Constantine (2018)) as implemented by the authors in the publicly available Python library. In all cases, Riemannian BFGS achieved better results.

For this example, we have chosen $p = 3$. We performed a sensitivity analysis on this parameter and found that a larger value might lead to better results in some cases but not in all cases. The full results are included in Appendix F. In that section, we also provide a sensitivity analysis to the starting point of the optimization. Since BFGS is quasi-Newton method, it is not guaranteed to find a global minimum in a general case. In the case of the polynomial basis with LDR, we find that the selection of the starting point makes a big difference in the final result.

Tables 4 and 5 show the results of applying LDR ($p = 3$) to the European call problem and we can see how this method performs in relation to the other alternatives. We can see that the polynomial LDR has lower error than nested Monte Carlo and both regress-now and regress-later polynomials. It also becomes clear that the LDR approach allows high dimensional problems where the regress-later approach on a full polynomial basis would fail.

4.2.3 Neural networks

In this section, we describe the results achieved using a neural network model as defined in Section 3.4. For this example we have chosen to work with 100 nodes, that is, the hidden layer is 100 nodes wide. This choice was made via cross-validation.

The neural network was optimized via backpropagation using the BFGS algorithm from Python’s popular library scikit-learn (Pedregosa et al. (2011)). The results in Tables 4 and 5 show an excellent quality of the neural network replicating martingale in this example, outperforming every other choice, except for the risk calculations with a very low number of samples (1,000).

In the comparison between neural network approaches, we can see that the replicating martingale—a regress-later method—outperforms the regress-now variation, the same way that it did for the polynomials.

In Figure 2 we can compare the empirical distribution for each method. This figure makes it easy to qualitatively assess the differences between the different methods, for example: the high variance of nMC vis-a-vis the lower variance of replicating martingales, or the higher accuracy of

regress-later methods compared to regress-now methods. We can also see that, despite the non-linear optimization with random starting points involved, the neural network replicating martingale does not have qualitatively higher variance than the polynomial equivalents.

It is interesting to consider the structure of the neural network and polynomial models, to understand what they have in common and what they do not. As seen in (5), both methods use a linear map to reduce the dimensionality of the input before applying a non-linear function. The polynomial model is based on global polynomials while the neural network can be seen as a data-driven piece-wise linear model. While usually piece-wise linear models require a grid to be defined a priori, neural networks adjust the bias term to “place” the grid where it is most needed according to the input data.

4.3 Comparison to lasso

The lasso (Tibshirani (1996)) is a popular model building technique for generating sparse models. It is used very successfully as a method for feature selection, especially in high dimensional problems. For that reason it is natural to compare the lasso regressor with the replicating martingale approach we present in this paper. At the same time, the comparison reveals the interesting differences in the way that replicating martingales and lasso perform the dimensionality reduction.

The lasso estimates of a linear model on a full polynomial bases, as in Section 3.2 are obtained by

$$\widehat{\beta} = \arg \min_{\beta} \|y - \Phi^\top \beta\|_{\mathbb{R}^n}^2 + \lambda \sum_{j=1}^m |\beta_j|.$$

One important difference is that lasso does not change the size of the regression problem, only the sparsity of the solution. Therefore the regression problem does not become smaller, unlike the case of polynomials with linear dimensionality reduction where once the input variables are projected, the remaining OLS problem is much smaller than the original.

A second important difference is that lasso selects among preexisting features, rather than creating new ones. The methods we described above create new features adaptively, under the assumption that the true function can be expressed in a low dimensional space. This lower dimension number p must be specified and becomes fixed, which is a disadvantage in respect with lasso which does not require a predetermined number of features. The ability to “create” new features gives the replicating martingale an advantage over lasso, which is limited to the input feature map. However, doing so while being faster in high-dimensional cases is part of what makes the replicating martingales an interesting method. The next section contains a comparison of runtime across different methods.

For this numerical example, the lasso estimator is built from the full polynomial basis—816 elements for $T = 5$ and 302,621 for $T = 40$. The feature map used for lasso is consequently the upper bound of the polynomial LDR feature map, that is, the one corresponding to $p = 15$ and $p = 120$ for $T = 5$ and $T = 40$ respectively. In the example we use $p = 3$, and therefore the success

of the polynomial LDR estimator will depend on whether a good solution can be expressed in the lower dimensional space of the resulting feature map.

To automate the selection of the penalty factor, we use the Akaike information criterion, using the algorithm provided by scikit-learn in its LassoLarsIC module, which is partly based on Zou, Hastie, Tibshirani, et al. (2007).

Table 7 shows the comparison between lasso and two replicating martingale methods—LDR and neural network—for both MApE and L_1 error. The quality of lasso is consistently worse than that of the other estimators, both in the tail and across the body of the distribution.

4.4 Comparison of runtime

The last comparison that we present on this European call example shows how long it takes to run the training and prediction phases on each model. This involves: running the regression on the number of samples indicated on the first column and calculating $\hat{Z}_1(x_i)$ for 1,000,000 validation samples.

The results are presented in Table 8. They clearly show the effect of the dimensionality reduction in the computational cost of the replicating martingale method. In high-dimensional problems, where the lasso regression must work with all features in the high-dimensional space, the LDR and Neural Network models are two orders of magnitude faster since the dimensionality reduction takes place prior to the creation of the features, thus creating a smaller regression problem.

5 Insurance liability model example

Having shown the effectiveness of learning the replicating martingale in the case of an European call, we present now a much more complex example: a variable annuity guarantee. Unlike the previous example, this one features path dependent cash flows at multiple points in time and also a dependency on a stochastic mortality model, rather than only stochastic market variables. The model has been built using models commonly in use in the insurance industry. The policyholder population is fictitious.

The example is constructed as follows. There are five stochastic drivers, $d = 5$: two for the interest rate model, one for the equity model, one for the real estate model, and one for the stochastic mortality. The interest rate and equity models are those described in Appendix B and used in previous examples. The real estate model is the same as the equity model from Appendix B, but uses an independent stochastic driver and a lower volatility than the equity model. The stochastic mortality follows a Lee–Carter model (R. D. Lee and Carter (1992)) to provide a trend and random fluctuations over time.

The insurance product being simulated is an investment account with a “return premium on death” guarantee. Every policyholder has an investment account. At each time period, the policyholders pay a premium, which is used to buy assets. These assets are deposited in the fund. The fund is re-balanced at each time period to maintain a target asset allocation. The value of the

fund is driven by the inflows from premiums and the market value changes, which are driven by the interest rate, equity, and real estate models. At each time step, a number of policyholders die—as determined by the stochastic life table—and the investment fund is paid out to the beneficiaries. If the investment fund were below the guaranteed amount, the company will additionally pay the difference between the fund value and the guaranteed amount. The guaranteed amount is the simple sum of all the premiums paid over the life of the policy. Over the course of the simulation the premiums paid gradually increase the guaranteed amount for each policy.

All policies have the same maturity date. In the short-term, low dimensional example, the maturity is $T = 5$. In the long term, high dimensional example the maturity is $T = 40$. At maturity, the higher of the fund value and the guaranteed amount is paid out to all survivors.

The investment portfolio holds four assets: a ten-year zero coupon bond, a twenty-year zero coupon bond, an equity index and a real estate index. The bonds are annually replaced such that the time to maturity remains constant.

The model is described by the following equations, where all financial variables are nominal amounts, unless otherwise noted:

Cash flows

- D_t : total dead in period $(t-1, t)$
- L_t : total of policyholders alive at time t
- A_t : value of assets at time t (per policy)
- G_t : guaranteed value at time t (per policy)
- C_t : value of the cash account at time t
- T : maturity date of the policies

$$\zeta_t = \begin{cases} D_t \max(A_t, G_t)/C_t, & t < T \\ L_{T-1} \max(A_T, G_T)/C_T, & t = T \end{cases}$$

In these equations, ζ_t is the only discounted variable—by the cash index—all other variable are nominal amounts.

Investment fund

- V_t^i : unit price of asset i at time t
- U_t^i : number of units of asset i held (per policy) in the fund at time t
- $B(t, S)$: value at time t of a bond maturing at time S
- EQ_t : value of equity index at time t
- RE_t : value of real estate at time t
- M : asset allocation mix
- P_t : premium paid (per policy) at time t

$$A_t = \sum_i U_t^i V_t^i$$

$$U_t^i = \begin{cases} U_{t-1}^i \frac{B(t, t+9)}{B(t, t+10)} + \frac{P_t M_i}{V_t^i}, & i = 1 \\ U_{t-1}^i \frac{B(t, t+19)}{B(t, t+20)} + \frac{P_t M_i}{V_t^i}, & i = 2 \\ U_{t-1}^i + \frac{P_t M_i}{V_t^i}, & i = 3, 4 \end{cases}$$

$$M = \left(\frac{1}{3}, \frac{1}{3}, \frac{1}{5}, \frac{2}{15} \right)$$

$$V_t^i = \begin{cases} B(t, t+10), & i = 1 \\ B(t, t+20), & i = 2 \\ EQ_t, & i = 3 \\ RE_t, & i = 4 \end{cases}$$

Bond prices (B), equity and real estate indices (EQ and RE) are simulated according to the model in Appendix B.

Policy variables

$$G_t = G_{t-1} + P_t$$

$$P_t = 100$$

$$G_0 = 100$$

Demographic variables

- D_t^x : total dead of age x in period $(t-1, t)$
- L_t^x : total alive of age x at time t
- $q_x(t)$: death rate for age x in period $(t-1, t)$

$$D_t = \sum_x D_t^x$$

$$D_t^x = L_{t-1}^x q_x(t)$$

$$L_0^x = 1000 \quad \forall x \in (30, 70)$$

Mortality model (Lee–Carter)

- $m_x(t)$: force of mortality at time t for age x
- a_x and b_x : Lee–Carter parameters (table in Appendix E)
- $X_t^{(lc)}$: element of innovation process X at time t used for mortality model

$$q_x(t) = 1 - e^{-m_x(t)}$$

$$m_x(t) = e^{a_x + b_x k(t)}$$

$$k(t) = k(0) - 0.365t + \epsilon_t$$

$$\epsilon_t = 0.621 X_t^{(lc)} \sqrt{t}$$

$$k(0) = -11.41$$

5.1 Results

The results for the variable annuity guarantee confirm those of European option case: the replicating martingale works very well, in particular the neural network model, which provides the best results in most cases. However, the more complex example also shows some limitations of the methods.

In the estimation of the present value (Table 9) we can observe:

- Monte Carlo simulation is still very effective, but regression-based methods provide slightly better accuracy.
- The neural network model performs relatively badly in the case with the lowest number of samples (1,000) and high dimensions ($T = 40$), providing the worst results in that case. This is driven by over-fitting, as we describe in the analysis of the mean relative L_1 error below. The quality reaches that of the other methods as the number of samples increase.
- The polynomial LDR method—which is calculated with $p = 10$ —shows its advantage over the full polynomial basis not only in being able to solve the high dimensional case, but also in the estimation of the low dimensional case with low number of samples. The full polynomial basis has a MApE of 61% due to the basis containing $\binom{25+3}{25} = 3,276$ elements, which exceeds the 1,000 available samples. The polynomial LDR has a MApE of less than 0.1% due to only containing 286 basis elements.

In the estimation of the expected shortfall (Table 10 and Figure 3) and the analysis of the mean relative L_1 error (Table 11) we can observe:

- Regress-later methods dominate over regress-now methods and nested Monte Carlo, with better mean absolute error and standard deviation.
- Unlike the case in the European call example where neural networks completely dominated the quality comparison, polynomial LDR shows better results in a few cases. However, which method shows better results is very sensitive to the choice of hyper-parameters. We provide a sensitivity analysis for hyper-parameters in Appendices F and G. Overall, neural networks have more room for improvement with an alternative choice of hyper-parameters and can be assumed to produce better results in this variable annuity example.
- We can observe several cases where an insufficient number of training samples leads to over-fitting and poor out-of-sample results. For example, for the full polynomial basis and $T = 5$, we find a large improvement in results when the training data changes from 1,000 samples to 5,000 samples. This basis has $m = 3,276$ which means that when working with 1,000 samples we have more parameters than samples. The same effect can be seen in the neural network replicating martingale for $T = 40$ when the sample size changes from 10,000 to 50,000 samples. This can be explained by the fact that this model has 20,201 parameters.
- In some cases, for example, the case neural network regress-later estimator for $T = 5$ the MApE ES increases when the sample size increases from 5,000 to 10,000 and 50,000 (Table 10). This behaviour is not present in the relative mean L_1 error (Table 11). This is due to the divergence between the error being minimized—errors along the full cash flows distribution—and the error being measured—errors in the tail of $T = 1$ conditional expectation distribution.

5.2 Comparison of runtime

The comparison of runtime for the insurance example is very important to determine the relative strength of the methods as feasible solution in the real world. For the reasons described in the introduction, nested Monte Carlo is not a feasible method for this problem, and it is therefore excluded from this comparison.

Unsurprisingly, we find regress-now methods to be faster than regress-later methods. This might partially explain the popularity with practitioners, especially for frequent calculations that do not require high precision. However, for quarterly or annual calculations of regulatory solvency, it seems hard to justify the much higher error rates for the benefit of saving a few minutes of calculations.

The slowest method is the polynomial LDR, which for the high dimensional problem takes almost 25 minutes to find the solution and make the estimation of the out-of-sample distribution. This time is entirely dominated by the optimization—training—step, not the estimation—prediction—step. The polynomial LDR method runtime is extremely sensitive to the p parameter. For example, for $T = 40$ and sample size 1,000, it takes 33 seconds to solve with $p = 5$ and 279.1 seconds to solve with $p = 10$.

The neural network model can be solved relatively fast, taking 2 minutes in the largest problem.

6 Conclusions

In the context of the need for accurate and fast calculations in portfolio pricing and risk management, we have introduced a data-driven method to build replicating martingales under different functional bases. This method yields lower errors than standard nested Monte Carlo simulation.

The model learns the features necessary for an effective low-dimensional representation from finite samples in a supervised setting. By doing so, it can be very effective in high-dimensional problems, without some of the usual difficulties associated with them.

We have presented two examples to demonstrate the usefulness of replicating martingales in the calculation of economic capital. The first is a typical benchmark example for calculations involving financial derivatives: an European call option. The second is a path-dependent insurance product, a variable annuity guarantee. Replicating martingales outperform other methods in the literature and in use in the financial industry for these two representative cases. This is illustrated by extensive comparisons and sensitivity analyses.

Appendix

A Quality metrics

Since the focus on this paper are applications in pricing and risk managements, we use two key quality metrics. The first one looks into the goodness of fit in the tail of the distribution, and the second one the goodness of fit across the body of the distribution.

For the tail of the distribution we look at expected shortfall and value at risk, for the loss-making tail. For the body of the distribution we look at the L_1 error.

We treat the models as statistical estimators since their estimates are subject to the randomness of their inputs. For that reason, for each those metrics described above we derive an empirical distribution based on R macro-runs of the the entire simulation-estimation-prediction chain of calculations. That means that we also need to define which metric summarizes the results of the empirical distribution. In both cases (tail error and L_1 error) we use the mean absolute error. In all cases we work with relative errors, expressed as a percentage. Root mean squared errors would have been an option but the advantages of the mean absolute error have been well documented in Willmott and Matsuura (2005) and Chai and Draxler (2014).

In the sections below we describe in detail the calculation of our two quality metrics: mean absolute percentage error on tail error (MApE), and mean relative L_1 error.

A.1 Mean absolute percentage error

Let us consider an empirical distribution of $X_{1:t}$, composed of n samples. From this distribution we can obtain an empirical distribution of Z_t . Given a function f^* , we obtain R repetitions of its finite sample estimator \hat{f} . For each function in these $\{\hat{f}_j\}_{j=1}^R$, we can produce an empirical distribution of its value estimator $\hat{Z}_t = \mathbb{E}_t^Q[\hat{f}(X)]$ using $X_{1:t}$, therefore obtaining a set of empirical distributions $\{\hat{Z}_t^{(j)}\}_{j=1}^R$.

Given a benchmark expected shortfall calculation at α (e.g., 99%) confidence, $\text{ES}_\alpha[-\Delta Z_t]$, an estimator of such quantity $\text{ES}_\alpha[-\Delta \hat{Z}_t^{(j)}]$, and R repetitions (independent samples) of such estimator $j = 1 \dots R$, the mean absolute percentage error (MApE) is defined as

$$\text{MApE ES} = \frac{1}{R} \sum_{j=1}^R \frac{|\text{ES}_\alpha[-\Delta \hat{Z}_t^{(j)}] - \text{ES}[-\Delta Z_t]|}{\text{ES}[-\Delta Z_t]}.$$

The MApE metric can also be applied to the present value of Z_t , $\mathbb{E}[Z_t] = Z_0$:

$$\text{MApE PV} = \frac{1}{R} \sum_{j=1}^R \frac{|\hat{Z}_0^{(j)} - Z_0|}{Z_0}.$$

A.2 Mean relative L_1 error

Given the above, the mean relative L_1 error is defined as

$$\frac{1}{R} \sum_{j=1}^R \frac{\mathbb{E}[|\hat{Z}_t^{(j)} - Z_t|]}{\mathbb{E}[|Z_t|]}$$

This metric is related to the error on the expected shortfall in the following way

$$|\text{ES}_\alpha[\hat{Z}_t] - \text{ES}_\alpha[Z_t]| \leq \frac{1}{\alpha} \mathbb{E}[|\hat{Z}_t - Z_t|].$$

This shows that for any α , the expected shortfall MApE is bounded by a multiple of the L_1 error. While the MApE ES is a metric calculated for a particular α and only takes into account the distribution beyond the α -th percentile, the mean relative L_1 error takes into account the whole distribution and bounds the expected shortfall error for any α .

B Economic scenario generator

B.1 Interest rate model

To model interest rates we use the one-factor Hull White model:

$$dr(t) = \alpha(b(t) - r(t))dt + \sigma dW(t).$$

B.2 Bond prices

The nominal price at time t of a zero-coupon bond with maturity T is given by

$$B(t, T) = \exp(-A(t, T)r(t) + C(t, T)) \quad (12)$$

where

$$\begin{aligned} A(t, T) &= \frac{1}{\alpha}(1 - e^{-\alpha(T-t)}), \\ C(t, T) &= -\alpha \int_t^T \int_t^u e^{-\alpha(u-s)} b(s) ds du + \frac{\sigma^2}{2\alpha^2} \left[(T-t) + \frac{1}{2\alpha}(1 - e^{-2\alpha(T-t)}) + \frac{2}{\alpha}(e^{-\alpha(T-t)} - 1) \right]. \end{aligned}$$

If we define $h(t, T) := \int_t^T \int_t^u e^{-\alpha(u-s)} b(s) ds du$ then

$$\begin{aligned} B(0, 1) &= \exp(-A(0, 1)r(0) + C(0, 1)) \\ &= \frac{1}{\alpha}(1 - \exp(-\alpha)) * r(0) - \alpha h(0, 1) + \frac{\sigma^2}{2\alpha^2} \left[1 + \frac{1}{2\alpha}(1 - e^{-2\alpha}) + \frac{2}{\alpha}(e^{-\alpha} - 1) \right]. \end{aligned} \quad (13)$$

Additionally, we define for future use

$$\begin{aligned} g(t) &:= \int_t^{t+1} e^{-\alpha(t+1-s)} b(s) ds \\ h(t) &:= h(t, t+1). \end{aligned}$$

B.3 Simulation

We simulate the short rate, r , and log-cash account, Y , jointly from Hull White one-factor model according to the formulas in Glasserman (2013), using the innovation process X as a stochastic driver.

$$Y(t) = \int_0^t r(u)du$$

$$\mu(t_i, t_i + 1) = \alpha \int_{t_i}^{t_i+1} e^{-\alpha(t_i+1-s)} b(s) ds = \alpha g(t_i) = \mu(t_i)$$

$$\sigma_r(t_i, t_i + 1) = \frac{\sigma^2}{2\alpha} (1 - e^{-2\alpha(t_i+1-t_i)}) = \frac{\sigma^2}{2\alpha} (1 - e^{-2\alpha}) = \sigma_r$$

$$r(t_i + 1) = e^{-\alpha(t_{i+1}-t_i)} r(t_i) + \mu(t_i, t_{i+1}) + \sigma_r(t_i, t_{i+1}) X_{i+1,1} = e^{-\alpha} r(t_i) + \mu(t_i) + \sigma_r X_{i+1,1}$$

$$\sigma_Y(t_i, t_{i+1}) = \frac{\sigma^2}{\alpha^2} \left((t_{i+1} - t_i) + \frac{1}{2\alpha} (1 - e^{-2\alpha(t_{i+1}-t_i)}) + \frac{2}{\alpha} (e^{-\alpha(t_{i+1}-t_i)} - 1) \right)$$

$$= \frac{\sigma^2}{\alpha^2} \left(1 + \frac{1}{2\alpha} (1 - e^{-2\alpha}) + \frac{2}{\alpha} (e^{-\alpha} - 1) \right) = \sigma_Y$$

$$\sigma_{rY}(t_i, t_{i+1}) = \frac{\sigma^2}{2\alpha} (1 + e^{-2\alpha(t_{i+1}-t_i)} - 2e^{-\alpha(t_{i+1}-t_i)}) = \frac{\sigma^2}{2\alpha} (1 + e^{-2\alpha} - 2e^{-\alpha}) = \sigma_{rY}$$

$$\rho_{rY}(t_i, t_{i+1}) = \sigma_{rY}(t_i, t_{i+1}) / [\sigma_r(t_i, t_{i+1}) \sigma_Y(t_i, t_{i+1})] = \sigma_{rY} / (\sigma_r \sigma_Y) = \rho_{rY}$$

$$X'_{i+1,2} = \rho_{rY} X_{i+1,1} + \sqrt{1 - \rho_{rY}^2} X_{i+1,2}$$

$$\mu_Y(t_i, t_{i+1}) = (1/\alpha) (1 - e^{-\alpha(t_{i+1}-t_i)}) r(t_i) + \alpha \int_{t_i}^{t_{i+1}} \int_{t_i}^u e^{-\alpha(u-s)} b(s) ds du$$

$$= (1/\alpha) (1 - e^{-\alpha}) r(t_i) + \alpha h(t_i) = \mu_Y(t_i)$$

$$Y(t_{i+1}) = Y(t_i) + \mu_Y(t_i) + \sigma_Y X'_{i+1,2}$$

B.4 Equity model

A geometric brownian process S_t models the equity excess return, therefore the equity index EQ_t is given by $EQ_t = C_t S_t$ where $C_t = \exp(Y(t))$ is the cash account.

We use this model for simulating for equity and real estate indices, with the recursive formula

$$S_t = S_{t-1} \exp \left(-\frac{\sigma^2}{2} + \sigma X'_{t,j} \right),$$

where $j = 3$ for the equity index and $j = 4$ for the real estate index. For a given Σ matrix that encodes the desired correlations, X' is a (correlated) innovation process $X'_t = \Sigma X_t$. For the examples in this paper, we have not been calibrated Σ to market data. In order to produce X' we set $X'_{t,1} = X_{t,1}$, $X'_{t,2}$, $X'_{t,3}$, $X'_{t,4}$ to be correlated with $X_{t,1}$ and $X'_{t,5} = X_t^{(lc)}$ —used for the mortality model—to be independent of all other variables.

C Proof of Theorem 1

Theorem 1 follows from Lemma 2 below by choosing $\tilde{A} = A(A^\top A)^{-1/2}$, which lies in $V_k(\mathbb{R}^{Td})$.

Lemma 2. *Let $A, \tilde{A} \in \mathbb{R}^{Td \times k}$ with full rank. The following are equivalent:*

1. $\text{Im } A = \text{Im } \tilde{A}$
2. $A = \tilde{A}S$, for some invertible $k \times k$ -matrix S
3. $\text{span } \phi_A = \text{span } \phi_{\tilde{A}}$

Proof. 1 \Leftrightarrow 2: is elementary.

2 \Rightarrow 3: define $\tilde{q}_i(y) = q_i(S^\top y)$ and note that $\{\tilde{q}_1, \dots, \tilde{q}_m\}$ is a basis of $\text{Pol}_\delta(\mathbb{R}^p)$. Note also that $\phi_{A,i}(x) = q_i(S^\top \tilde{A}^\top x) = \tilde{q}_i(\tilde{A}^\top x)$, while $\phi_{\tilde{A},i}(x) = q_i(\tilde{A}^\top x)$. This yields the claim.

3 \Rightarrow 1: as $\text{Pol}_\delta(\mathbb{R}^p)$ contains all linear polynomials on \mathbb{R}^p , we infer that for any $v \in \mathbb{R}^p$ there exists some $\tilde{v} \in \mathbb{R}^p$ such that $v^\top A^\top x = \tilde{v}^\top \tilde{A}^\top x$, for all $x \in \mathbb{R}^{Td}$, and vice versa. This completes the proof. \square

D Expectations under polynomial LDR

If $x \in \mathbb{R}^p$, $H_\alpha(x)$ for $\alpha \in \mathbb{N}_0^p$ is a multivariate Hermite polynomial of order α_j in the j -th dimension.

Lemma 3. *Given $\underline{X} \sim N(0, I_{Td})$ and $A \in V_p(\mathbb{R}^{Td})$, the conditional expectation of the Hermite polynomial of order α is*

$$\mathbb{E}_t[H_\alpha(A^\top \underline{X})] = \prod_{j=1}^p \sigma[W_j^-]^{\alpha_j} H_{\alpha_j} \left(\frac{W_j^-}{\sigma[W_j^-]} \right) \quad (14)$$

where $\sigma[W_j^-] = \sqrt{\sum_{s=1}^{Td} A_{sj}^2}$.

Proof. Since $A^\top \underline{X} \sim N(0, I_p)$, we have

$$\mathbb{E}_t[H_\alpha(A^\top \underline{X})] = \mathbb{E}_t \left[\prod_{j=1}^p H_{\alpha_j}(A_j^\top \underline{X}) \right] = \prod_{j=1}^p \mathbb{E}_t \left[H_{\alpha_j}(A_j^\top \underline{X}) \right]. \quad (15)$$

At this point we separate those terms before and including t and those after t , and define $W_j^- = \sum_{s=1}^{Td} A_{sj} \underline{X}_s$ and $W_j^+ = \sum_{s=td+1}^{Td} A_{sj} \underline{X}_s$, so that W_j^- is \mathcal{F}_t -measurable, W_j^+ is independent of \mathcal{F}_t , and $A_j^\top \underline{X} = W_j^- + W_j^+$.

To continue the proof, we introduce the Hermite polynomials of variance ν , $H_n^{[\nu]}(x) = \nu^{\frac{n}{2}} H_n\left(\frac{x}{\sqrt{\nu}}\right)$ following Roman (1984), Section 2.1. These generalized Hermite polynomials form an Appell sequence for which the following identity holds (Equation 4.2.1 in Roman (1984)):

$$H_n^{[\nu+\mu]}(x+y) = \sum_{k=0}^n \binom{n}{k} H_k^{[\nu]}(x) H_{n-k}^{[\mu]}(y).$$

This is the binomial convolution of $H_k^{[\nu]}$ and $H_{n-k}^{[\mu]}$ under umbral calculus.

Note that the variance of $W_j^- + W_j^+$ fulfills

$$\sigma^2[W_j^- + W_j^+] = \sigma^2[W_j^-] + \sigma^2[W_j^+] = 1.$$

Setting $\nu = \sigma^2[W_j^-]$ and $\mu = \sigma^2[W_j^+]$ we obtain

$$\begin{aligned} H_{\alpha_j}(W_j^- + W_j^+) &= H_{\alpha_j}^{[\sigma^2[W_j^-] + \sigma^2[W_j^+]]}(W_j^- + W_j^+) \\ &= \sum_{k=0}^{\alpha_j} \binom{\alpha_j}{k} H_k^{[\sigma^2[W_j^-]]}(W_j^-) H_{\alpha_j-k}^{[\sigma^2[W_j^+]]}(W_j^+) \\ &= \sum_{k=0}^{\alpha_j} \binom{\alpha_j}{k} \sigma[W_j^-]^k H_k\left(\frac{W_j^-}{\sigma[W_j^-]}\right) \sigma[W_j^+]^{\alpha_j-k} H_{\alpha_j-k}\left(\frac{W_j^+}{\sigma[W_j^+]}\right). \end{aligned}$$

Applying the \mathcal{F}_t -conditional expectation, we obtain

$$\mathbb{E}_t \left[H_{\alpha_j}(W_j^- + W_j^+) \right] = \sum_{k=0}^{\alpha_j} \binom{\alpha_j}{k} \sigma[W_j^-]^k H_k\left(\frac{W_j^-}{\sigma[W_j^-]}\right) \sigma[W_j^+]^{\alpha_j-k} \mathbb{E}_t \left[H_{\alpha_j-k}\left(\frac{W_j^+}{\sigma[W_j^+]}\right) \right],$$

since

$$\mathbb{E}_t \left[H_k\left(\frac{W_j^-}{\sigma[W_j^-]}\right) \right] = \mathbb{E} \left[H_k\left(\frac{W_j^-}{\sigma[W_j^-]}\right) | W_j^- \right] = H_k\left(\frac{W_j^-}{\sigma[W_j^-]}\right).$$

Replacing in (15), and taking into account that

$$\sigma[W_j^+]^{\alpha_j-k} \mathbb{E}_t \left[H_{\alpha_j-k}\left(\frac{W_j^+}{\sigma[W_j^+]}\right) \right] = \begin{cases} 0 & \forall k \neq \alpha_i \\ 1 & k = \alpha_i \end{cases},$$

we obtain (14). \square

E Lee–Carter parameters

The Lee–Carter parameters are based on the findings in the original paper R. D. Lee and Carter (1992), and they are shown in Table 13.

F Sensitivity of polynomial LDR to hyper-parameters

The polynomial LDR method has two hyper-parameters, the target dimensionality p and the polynomial degree δ . Additionally, the Riemannian BFGS algorithm used to solve the optimization problem adds several other parameters, the main one being the starting point for the parameter A , called here A_0 .

The polynomial degree parameter is common to all polynomial approximations, and has the expected impact on the results. In this section, we focus on the parameter p which is unique to the linear dimensionality reduction and the parameter A_0 which in our empirical examples proved to have a large impact on results.

We show that the choice of p is purely a trade-off between approximation error and number of samples required, and that the choice of starting point makes a very large difference in the final results. A random starting point performs relatively badly, compared to a starting point that takes into account the fact that in financial models, cash flows closer in time are usually more important than those farther in time.

F.1 Starting point A_0

The Riemannian BFGS algorithm used to solve the polynomial LDR optimization problem requires a starting point for A .

A simple way of generating a starting point—similar to what is done for the L-BFGS algorithm used to solve the neural network optimization problem—is to generate it randomly. To do this we draw Tdp random samples from $N(0, 1)$ and arrange them into an $Td \times p$ matrix B . Then $A_0 = B(B^\top B)^{-1/2}$ is a random matrix that follows the uniform distribution on the Stiefel manifold $V_p(\mathbb{R}^{Td})$.

A second way is to use a rectangular diagonal matrix and fill the last column to ensure that every one of the Td input dimensions has a weight in at least one of the p output dimension, that is $A_0 = B \mid B_{ij} = 1$ if $(i = j \wedge i \neq p) \wedge B_{ip} = \frac{1}{\sqrt{Td-p+1}}$ if $i \geq p$. Conceptually, this starting point can be thought as a point where those input dimensions farthest in the future have been grouped into one output dimension. The following is an example for $Td = 4$ and $p = 3$:

$$\begin{pmatrix} 1 & 0 & 0 \\ 0 & 1 & 0 \\ 0 & 0 & \sqrt{0.5} \\ 0 & 0 & \sqrt{0.5} \end{pmatrix}.$$

A third way uses the same rationale of grouping input dimensions that are far in the future into one output dimension, but does so respecting the fact that $X \in \mathbb{R}^{T \times d}$ and only groups variables across time (T) but not across dimensions (d). The following is an example for $T = 5$, $d = 3$ and $p = 3$ which corresponds to what was used in the European call example in Section 3.3:

$$\begin{pmatrix} \sqrt{T} & 0 & 0 \\ 0 & \sqrt{T} & 0 \\ 0 & 0 & \sqrt{T} \\ \vdots & \vdots & \vdots \\ \sqrt{T} & 0 & 0 \\ 0 & \sqrt{T} & 0 \\ 0 & 0 & \sqrt{T} \end{pmatrix}.$$

Since this method, which we call “folding”, provides the best results we also use it in Sections 4 and 5. In the latter we work with $T = 5$, $d = 5$ and $p = 10$, and leads to a starting point (in block notation):

$$\begin{pmatrix} \mathbf{1}_d & \mathbf{0}_{d \times (p-d)} \\ \mathbf{0}_{d \times d} & \sqrt{T-1} \mathbf{1}_{p-d} \\ \vdots & \vdots \end{pmatrix} \} T-1 \text{ times}.$$

In Tables 14 and 15 we can see the comparison across different starting points. The folding starting point performs best of all starting points. This is not surprising since it is expected that for this type of models—financial derivatives and insurance liabilities—the combination of path dependency and discounting makes variables closer in time relatively more important than those farther in time. A disappointing characteristic revealed in the data is that when increasing the number of training samples, we do not always get a strictly decreasing error. In fact, the error seems to stabilize relatively early—around 5000 samples—and then only be subject to small fluctuations. The comparison across starting points confirms that this lack of improvement is not due to a lack of a better solution, but rather most likely to the presence of local minima.

F.2 Target dimensionality parameter p

To show the effects of parameter p on the insurance example, we choose one of the starting point methods (diagonal) and one maturity ($T = 5$). The results in Tables 16 and 17 confirm the expected effect of changing this parameter: larger values of p produce better results (since f^* is a richer function) but also require more training samples to do so. We can see that when moving from $p = 10$ —used in the main results for the insurance example—to $p = 15$ and therefore from $m = 286$ to $m = 816$ the error for 1,000 training samples increases by a factor of 10 in the expected shortfall and by a factor of 3 in the L_1 metric. In those cases with more training samples—5,000 and above—the error goes down as expected.

G Sensitivity of neural network to hyper-parameters

The neural network method has one main hyper-parameter, the width of the hidden layer. Other typical neural network hyper-parameters as number of layers or activation function do not apply in this case, since the closed-form of the time- t expectation has been defined only for single-layer, ReLu networks. Unlike the polynomial LDR basis, we do not explore the impact of the starting point, since a random starting point already performs very well.

In the main results in Section 5, we use the same layer width in all cases, $p = 100$. This value is the results of a sensitivity test done for different values (10, 50, 100, 200) after which we chose the best results overall cases. This sensitivity test is similar to cross validation but is performed on entirely out-of-sample data, rather than partitioning the existing training data. Using a single choice of layer width in all cases has the advantage of showing good overall results (for different maturities and training sample size) but the disadvantage of being neither optimized for each single case (meaning that the results could have been better when looking at each cell of the table) nor comparable to the polynomial method in terms of functional complexity, that is, the number of parameters that describe the function f^* .

The selection could have been done in different ways, and in this section we show some alternatives and their effects on the results shown in Section 5. The results are summarized in Tables 18 and 19. We show that some of the alternatives perform even better than our choice for the main results, implying the potential for improvement in the neural network basis, which is already the best performing basis in our comparisons.

The first alternative is to use the theoretical minimum width for the network, as described in Hanin and Sellke (2017). In our case, it means using $p = 25$ for $T = 5$ and $p = 200$ for $T = 40$. This method does not show a good performance. Interestingly, it performs worse even for $T = 40$ where $p = 100$ is below the minimum. Still, this is not a violation of the theoretical minimum since this is valid for neural networks of arbitrary length, so it is always possible that using more hidden layers would result in smaller errors than the fixed p method.

The second alternative is to backsolve the width of the network that creates a parameter space of similar dimensionality as that of the polynomial LDR method. For $d = 5$, $T = 5$ and $p = 10$ the polynomial LDR has 481 parameters. For $T = 40$ it has 2,231 parameters. This can be matched by using a neural network with $p = 18$ and $p = 11$ nodes respectively. This alternative provide very good results for the high dimensionality case ($T = 40$) but not as good for the low dimensionality case ($T = 5$).

The third and final alternative is to use a neural network that matches the number of basis functions m . This means, for both $T = 5$ and $T = 40$, that $p = 286$. The results for this alternative are similar to the other alternatives.

References

Absil, P-A, Christopher G Baker, and Kyle A Gallivan (2007). “Trust-region methods on Riemannian manifolds”. In: *Foundations of Computational Mathematics* 7(3), pp. 303–330 (cit. on p. 15).

Andreatta, Giulia and Stefano Corradin (2003). “Valuing the surrender options embedded in a portfolio of italian life guaranteed participating policies: a least squares Monte Carlo approach”. In: *Proceedings of “Real option theory meets practice”, 8th Annual International Conference, Montreal* (cit. on p. 3).

Broadie, Mark, Yiping Du, and Ciamac C Moallemi (2015). “Risk estimation via regression”. In: *Operations Research* 63(5), pp. 1077–1097 (cit. on pp. 3, 13).

Carriere, Jacques F (1996). “Valuation of the early-exercise price for options using simulations and nonparametric regression”. In: *Insurance: mathematics and Economics* 19(1), pp. 19–30 (cit. on p. 3).

Castellani, Gilberto et al. (2018). “An investigation of Machine Learning Approaches in the Solvency II Valuation Framework”. In: *Available at SSRN 3303296* (cit. on p. 4).

Chai, Tianfeng and Roland R Draxler (2014). “Root mean square error (RMSE) or mean absolute error (MAE)?–Arguments against avoiding RMSE in the literature”. In: *Geoscientific model development* 7(3), pp. 1247–1250 (cit. on p. 22).

Cunningham, John P and Zoubin Ghahramani (2015). “Linear dimensionality reduction: Survey, insights, and generalizations”. In: *The Journal of Machine Learning Research* 16(1), pp. 2859–2900 (cit. on p. 9).

Fernandez-Arjona, Lucio (2019). “A neural network model for solvency calculations in life insurance”. In: arXiv: 2005.02318 [q-fin.CP] (cit. on p. 11).

Fernandez-Arjona, Lucio and Damir Filipović (2020). *Benchmark and training data for replicating financial and insurance examples*. Zenodo. DOI: [10.5281/zenodo.3837381](https://doi.org/10.5281/zenodo.3837381) (cit. on p. 3).

Glasserman, Paul (2013). *Monte Carlo methods in financial engineering*. Vol. 53. Springer Science & Business Media (cit. on p. 24).

Glasserman, Paul and Bin Yu (2002). “Simulation for American options: Regression now or regression later?” In: *Monte Carlo and Quasi-Monte Carlo Methods 2002*. Springer, pp. 213–226 (cit. on pp. 2, 3, 6).

Gordy, Michael B and Sandeep Juneja (2010). “Nested simulation in portfolio risk measurement”. In: *Management Science* 56(10), pp. 1833–1848 (cit. on p. 4).

Hanin, Boris and Mark Sellke (2017). “Approximating continuous functions by relu nets of minimal width”. In: *arXiv preprint arXiv:1710.11278* (cit. on p. 29).

Hokanson, Jeffrey M and Paul G Constantine (2018). “Data-driven polynomial ridge approximation using variable projection”. In: *SIAM Journal on Scientific Computing* 40(3), A1566–A1589 (cit. on pp. 4, 6, 15).

Huang, Wen, Kyle A Gallivan, and P-A Absil (2015). “A Broyden class of quasi-Newton methods for Riemannian optimization”. In: *SIAM Journal on Optimization* 25(3), pp. 1660–1685 (cit. on p. 15).

Lee, Ronald D. and Lawrence R. Carter (1992). “Modeling and Forecasting U. S. Mortality”. In: *Journal of the American Statistical Association* 87(419), pp. 659–671 (cit. on pp. 17, 27).

Lee, Shing-Hoi and Peter W Glynn (2003). “Computing the distribution function of a conditional expectation via Monte Carlo: Discrete conditioning spaces”. In: *ACM Transactions on Modeling and Computer Simulation (TOMACS)* 13(3), pp. 238–258 (cit. on p. 4).

Longstaff, Francis A. and Eduardo S. Schwartz (2001). “Valuing American Options by Simulation: A Simple Least-Squares Approach”. In: *The Review of Financial Studies* 14(1), pp. 113–147 (cit. on p. 3).

Madan, Dilip B and Frank Milne (1994). “Contingent claims valued and hedged by pricing and investing in a basis”. In: *Mathematical Finance* 4(3), pp. 223–245 (cit. on p. 3).

Pedregosa, F. et al. (2011). “Scikit-learn: Machine Learning in Python”. In: *Journal of Machine Learning Research* 12, pp. 2825–2830 (cit. on p. 15).

Pelsser, Antoon and Janina Schweizer (2016). “The difference between LSMC and replicating portfolio in insurance liability modeling”. In: *European actuarial journal* 6(2), pp. 441–494 (cit. on pp. 3, 4).

Roman, Steven (1984). *The umbral calculus*. Academic Press: New York. ISBN: 9780125943802 (cit. on p. 26).

Tibshirani, Robert (1996). “Regression shrinkage and selection via the lasso”. In: *Journal of the Royal Statistical Society: Series B (Methodological)* 58(1), pp. 267–288 (cit. on p. 16).

Townsend, James, Niklas Koep, and Sebastian Weichwald (2016). “Pymanopt: A python toolbox for optimization on manifolds using automatic differentiation”. In: *The Journal of Machine Learning Research* 17(1), pp. 4755–4759 (cit. on p. 15).

Willmott, Cort J and Kenji Matsuura (2005). “Advantages of the mean absolute error (MAE) over the root mean square error (RMSE) in assessing average model performance”. In: *Climate research* 30(1), pp. 79–82 (cit. on p. 22).

Zou, Hui, Trevor Hastie, Robert Tibshirani, et al. (2007). “On the degrees of freedom of the lasso”. In: *The Annals of Statistics* 35(5), pp. 2173–2192 (cit. on p. 17).

Table 1: Nested Monte Carlo, comparison of present value (50,000 total samples)

Maturity	Benchmark	nMC	MApE
5	22.1691	22.1806	0.6%
40	67.5488	67.5567	1.0%

Table 2: Nested Monte Carlo, comparison of expected shortfall for nested Monte Carlo (50,000 total samples)

Maturity	Benchmark (value)	Nested Monte Carlo (MApE by inner simulations)							
		1	10	25	50	100	250	400	500
5	56.8588	233.4%	29.5%	11.8%	7.9%	9.3%	14.4%	19.0%	20.4%
40	62.6205	2027.0%	463.6%	232.1%	129.2%	66.6%	24.6%	21.4%	19.1%

Table 3: Nested Monte Carlo, comparison of present value and expected shortfall MApE (in percentage points) for optimal inner–outer split

Samples	Present Value		Expected Shortfall	
	Maturity: 5	Maturity: 40	Maturity: 5	Maturity: 40
1,000	6.4	7.5	26.8	404.4
5,000	4.0	3.9	15.9	111.2
10,000	3.8	3.1	14.5	56.8
50,000	1.7	2.4	8.0	19.2

Table 4: European call, comparison of present value MAPE (in percentage points)

Samples	nMC	Full Polynomial basis		LDR Regress-later	Neural Network	
		Regress-now	Regress-later		Regress-now	Regress-later
T=5						
1,000	6.4	4.0	1.3	0.5	4.2	0.2
5,000	4.0	1.8	0.2	0.2	1.8	<0.1
10,000	3.8	1.2	0.1	0.1	1.2	<0.1
50,000	1.7	0.6	0.1	0.1	0.6	<0.1
T=40						
1,000	7.5	7.2		3.7	7.9	5.5
5,000	3.9	3.2		2.0	3.2	1.6
10,000	3.1	2.3		1.5	2.4	0.9
50,000	2.4	1.0		0.5	1.0	0.2

Table 5: European call, comparison of expected shortfall MAPE (in percentage points)

Samples	nMC	Full Polynomial basis		LDR Regress-later	Neural Network	
		Regress-now	Regress-later		Regress-now	Regress-later
T=5						
1,000	26.8	21.5	4.9	2.3	47.8	0.9
5,000	15.9	9.3	1.3	1.3	11.6	0.2
10,000	14.5	6.5	1.0	1.1	7.3	0.2
50,000	8.0	3.0	0.7	0.8	3.6	0.1
T=40						
1,000	404.4	141.4		10.2	459.9	16.0
5,000	111.2	47.0		6.2	107.2	4.9
10,000	56.8	29.7		4.9	57.5	3.3
50,000	19.2	12.6		2.9	11.5	0.9

Table 6: European call, comparison of relative mean L_1 error (in percentage points)

Samples	Full Polynomial basis		LDR Regress-later	Neural Network	
	Regress-now	Regress-later		Regress-now	Regress-later
T=5					
1,000	15.5	4.6	2.7	36.6	0.5
5,000	6.8	0.9	2.0	12.5	0.4
10,000	4.8	0.7	1.8	8.0	0.4
50,000	2.2	0.5	1.3	2.9	0.4
T=40					
1,000	26.5		4.5	68.8	7.4
5,000	11.9		2.6	24.0	2.2
10,000	8.5		2.0	14.9	1.4
50,000	3.9		1.4	4.1	0.8

Table 7: European call, comparison of MApE ES and relative mean L_1 error (both in percentage points)

Samples	MApE ES			Rel. mean L_1 error		
	Lasso	LDR	N. Net.	Lasso	LDR	N. Net.
T=5						
1,000	23.9	2.3	0.9	8.4	2.7	0.5
5,000	8.6	1.3	0.2	2.6	2.0	0.4
10,000	7.1	1.1	0.2	2.2	1.8	0.4
50,000	1.5	0.8	0.1	0.9	1.3	0.4
T=40						
1,000	100.0	10.2	16.0	64.2	4.5	7.4
5,000	83.9	6.2	4.9	24.7	2.6	2.2
10,000	70.7	4.9	3.3	17.9	2.0	1.4
50,000		2.9	0.9		1.4	0.8

Table 8: European call, comparison of runtime (in seconds), single core AMD Opteron 6380

Samples	Full Polynomial basis		LDR		Neural Network	
	Lasso	Regress-now	Regress-later	Regress-later	Regress-now	Regress-later
T=5						
1,000	1.7	0.9	1.5	1.4	9.5	18.4
5,000	3.4	0.9	2.3	1.6	16.1	21.1
10,000	6.1	0.9	3.0	2.1	24.0	24.4
50,000	24.9	1.0	13.4	7.1	92.6	49.4
T=40						
1,000	153.4	0.9		7.2	10.0	18.5
5,000	897.2	0.9		22.3	15.5	24.4
10,000	2,199.0	1.0		51.7	24.0	30.0
50,000		1.4		271.7	19.1	76.1

Table 9: Insurance liability, comparison of present value MAPE (in percentage points)

Samples	nMC	Full Polynomial basis		LDR Regress-later	Neural Network	
		Regress-now	Regress-later		Regress-now	Regress-later
T=5						
1,000	0.3	0.2	61.0	<0.1	0.3	0.1
5,000	0.3	0.1	<0.1	<0.1	0.1	<0.1
10,000	0.2	0.1	<0.1	<0.1	0.1	<0.1
50,000	0.1	<0.1	<0.1	<0.1	<0.1	<0.1
T=40						
1,000	0.5	0.5		0.2	0.6	6.2
5,000	0.3	0.2		0.1	0.2	0.3
10,000	0.3	0.2		0.1	0.2	0.4
50,000	0.2	0.1		<0.1	0.1	0.1

Table 10: Insurance liability, comparison of expected shortfall MAPE (in percentage points)

Samples	nMC	Full Polynomial basis		LDR Regress-later	Neural Network	
		Regress-now	Regress-later		Regress-now	Regress-later
T=5						
1,000	29.7	79.0	608.6	7.2	196.6	2.9
5,000	10.9	18.5	0.5	4.8	47.6	0.5
10,000	8.9	10.2	0.3	4.7	25.5	0.7
50,000	5.4	3.2	0.2	3.5	6.8	0.9
T=40						
1,000	106.1	228.6		25.4	524.4	14.8
5,000	33.4	64.8		5.5	149.0	11.1
10,000	19.3	36.3		7.8	85.7	10.5
50,000	11.0	10.2		7.4	13.2	0.5

Table 11: Insurance liability, comparison of relative mean L_1 error (in percentage points)

Samples	Full Polynomial basis		LDR Regress-later	Neural Network	
	Regress-now	Regress-later		Regress-now	Regress-later
T=5					
1,000	1.6	61.0	0.2	4.7	0.1
5,000	0.7	<0.1	0.2	1.6	0.1
10,000	0.5	<0.1	0.3	1.0	<0.1
50,000	0.2	<0.1	0.2	0.4	<0.1
T=40					
1,000	3.3		0.8	10.0	6.2
5,000	1.4		0.3	3.4	0.6
10,000	1.0		0.5	2.2	0.5
50,000	0.4		0.4	0.6	0.1

Table 12: *Insurance liability, comparison of runtime (in seconds), single core AMD Opteron 6380*

Samples	Full Polynomial basis		LDR	Neural Network	
	Regress-now	Regress-later	Regress-later	Regress-now	Regress-later
T=5					
1,000	0.8	4.3	30.4	4.0	5.5
5,000	0.9	54.4	113.2	11.1	8.2
10,000	1.1	45.3	49.6	19.8	11.9
50,000	3.0	108.1	238.6	95.1	42.7
T=40					
1,000	1.3		279.1	4.6	6.3
5,000	2.6		698.9	12.9	15.7
10,000	4.3		1,815.1	22.9	26.5
50,000	17.9		1,472.8	31.7	115.5

Table 13: Lee–Carter parameters a_x and b_x for every age x

x	a_x	b_x
0	-3.641090	0.90640
(1, 2, 3, 4)	-6.705810	0.11049
(5, 6, 7, 8, 9)	-7.510640	0.09179
(10, 11, 12, 13, 14)	-7.557170	0.08358
(15, 16, 17, 18, 19)	-6.760120	0.04744
(20, 21, 22, 23, 24)	-6.443340	0.05351
(25, 26, 27, 28, 29)	-6.400620	0.05966
(30, 31, 32, 33, 34)	-6.229090	0.06173
(35, 36, 37, 38, 39)	-5.913250	0.05899
(40, 41, 42, 43, 44)	-5.513230	0.05279
(45, 46, 47, 48, 49)	-5.090240	0.04458
(50, 51, 52, 53, 54)	-4.656800	0.03830
(55, 56, 57, 58, 59)	-4.254970	0.03382
(60, 61, 62, 63, 64)	-3.856080	0.02949
(65, 66, 67, 68, 69)	-3.473130	0.02880
(70, 71, 72, 73, 74)	-3.061170	0.02908
(75, 76, 77, 78, 79)	-2.630230	0.03240
(80, 81, 82, 83, 84)	-2.204980	0.03091
(85, 86, 87, 88, 89)	-1.799600	0.03091
(90, 91, 92, 93, 94)	-1.409363	0.03091
(95, 96, 97, 98, 99)	-1.036550	0.03091
(100, 101, 102, 103, 104)	-0.680350	0.03091
(105, 106, 107, 108)	-0.341050	0.03091

Table 14: Insurance liability, comparison of expected shortfall MAPE (in percentage points) for different starting points in polynomial LDR basis

Samples	Folding	Diagonal	Random
T=5			
1,000	7.2	19.1	18.5
5,000	4.8	16.6	30.8
10,000	4.7	22.5	31.1
50,000	3.5	30.1	32.1
T=40			
1,000	25.4	37.3	62.3
5,000	5.5	54.2	68.5
10,000	7.8	51.5	66.1
50,000	7.4	49.2	66.3

Table 15: Insurance liability, comparison of relative mean L_1 error (in percentage points) for different starting points in polynomial LDR basis

Samples	Folding	Diagonal	Random
T=5			
1,000	0.2	1.1	1.2
5,000	0.2	0.8	1.0
10,000	0.3	0.9	1.0
50,000	0.2	0.9	1.0
T=40			
1,000	0.8	1.8	1.7
5,000	0.3	1.3	1.5
10,000	0.5	1.3	1.5
50,000	0.4	1.2	1.6

Table 16: Insurance liability, comparison of expected shortfall MAPE (in percentage points) for different values of the target dimensionality parameter in polynomial LDR basis

Samples	Diagonal p=5	Diagonal p=10	Diagonal p=15	Diagonal p=20
T=5				
1,000	21.8	19.1	236.6	764.8
5,000	28.8	16.6	8.3	7.7
10,000	32.6	22.5	11.3	10.4
50,000	36.5	30.1	19.7	7.6

Table 17: Insurance liability, comparison of relative mean L_1 error (in percentage points) for different values of the target dimensionality parameter in polynomial LDR basis

Samples	Diagonal p=5	Diagonal p=10	Diagonal p=15	Diagonal p=20
T=5				
1,000	1.0	1.1	3.2	37.3
5,000	1.0	0.8	0.6	0.5
10,000	1.0	0.9	0.6	0.6
50,000	1.0	0.9	0.7	0.4

Table 18: Comparison of expected shortfall MAPE (in percentage points) for different layer widths in neural network basis

Samples	Fixed $p = 100$	Minimum width	Equal param dims	Equal m
T=5				
1,000	2.9	2.2	3.0	4.2
5,000	0.5	3.2	4.1	0.4
10,000	0.7	3.3	4.2	0.2
50,000	0.9	3.4	4.3	0.3
T=40				
1,000	14.8	14.5	17.2	13.7
5,000	11.1	12.2	2.6	12.5
10,000	10.5	12.4	1.9	12.6
50,000	0.5	1.5	2.1	2.4

Table 19: Comparison of relative mean L_1 error (in percentage points) for different layer widths in neural network basis

Samples	Fixed $p = 100$	Minimum width	Equal param dims	Equal m
T=5				
1,000	0.1	0.1	0.1	0.1
5,000	0.1	0.1	0.1	<0.1
10,000	<0.1	0.1	0.1	<0.1
50,000	<0.1	0.1	0.1	<0.1
T=40				
1,000	6.2	6.4	2.8	6.5
5,000	0.6	0.8	0.5	0.8
10,000	0.5	0.5	0.2	0.5
50,000	0.1	0.1	0.1	0.1

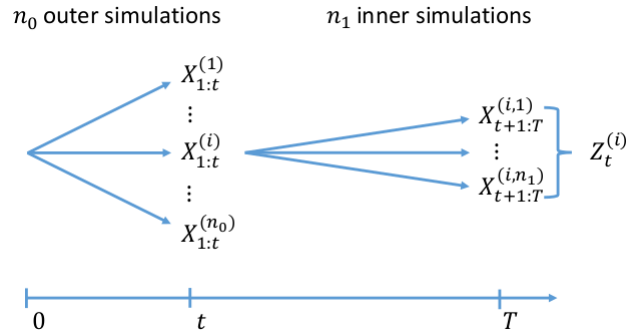


Figure 1: Nested Monte Carlo structure. The outer simulations span the time period 0 to t , and each of those serves as the starting point of a group of inner simulations.

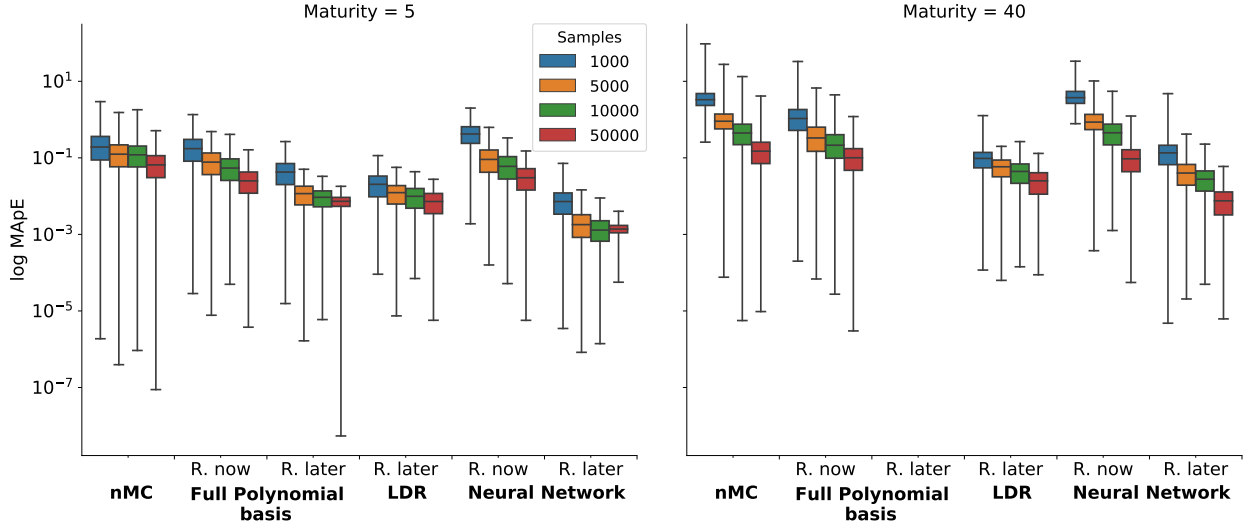


Figure 2: Distribution of expected shortfall estimates per method for the European call example. Boxes show the upper and lower quartiles of the empirical distributions, while whiskers show their maxima and minima. Due to the logarithmic scale, a visual artifact is introduced by which the inter-quartile range seems to increase with larger sample sizes—most notably in the nMC for Maturity=40. In reality, the inter-quartile range decreases with larger sample sizes, but the logarithmic scale makes the box bigger for smaller errors.

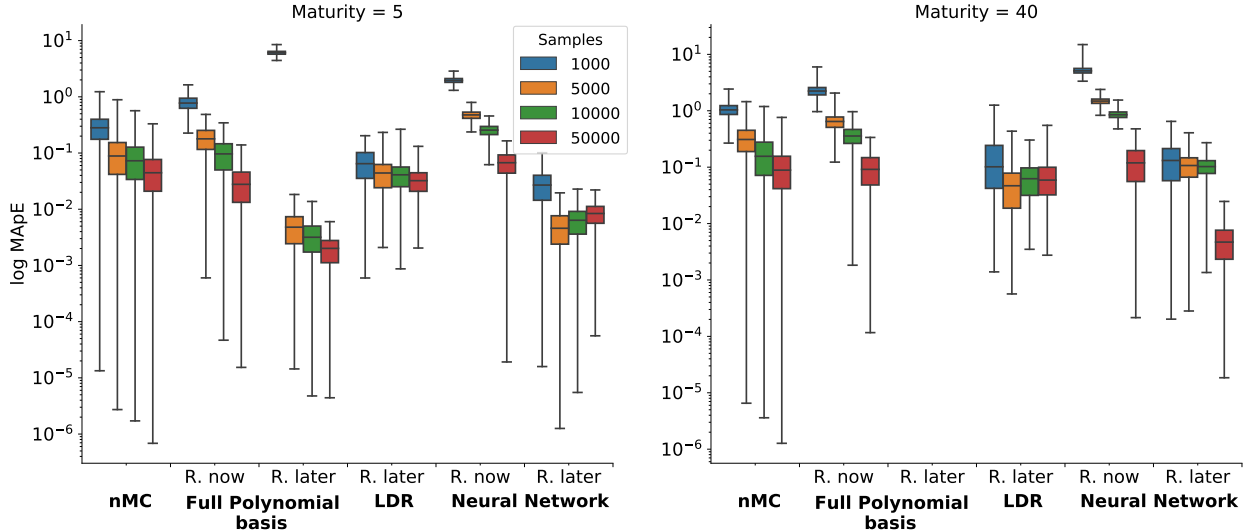


Figure 3: Distribution of expected shortfall estimates per method for the insurance liability example. Boxes show the upper and lower quartiles of the empirical distributions, while whiskers show their maxima and minima. Due to the logarithmic scale, a visual artifact is introduced by which the inter-quartile range seems to increase with larger sample sizes—most notably in the nMC for Maturity=40. In reality, the inter-quartile range decreases with larger sample sizes, but the logarithmic scale makes the box bigger for smaller errors.